RGNZ/MGPB

Rudarsko-geološko-naftni zbornik
(The Mining-Geology-Petroleum Engineering Bulletin)
DOI: 10.17794/rgn.2026.4.6

Original scientific paper

Modelling the effects of lateral loading on a bent strike-slip fault system: A case study from the Palu-koro and Matano faults, Indonesia

Dian Kusumawati[1,6], David P. Sahara[2], Nanang T. Puspito[2*], Mudrik R. Daryono[3], Andri D. Nugraha[2], Andrean V. H. Simanjuntak[4,5], Maulidia Ain Bening[2], Faiz Muttaqy[6]

[1] *Geophysical Engineering, Faculty of Mining and Petroleum Engineering, Institut Teknologi Bandung, Bandung 40132, Indonesia.*
[2] *Global Geophysics Research Group, Faculty of Mining and Petroleum Engineering, Institut Teknologi Bandung, Bandung 40132, Indonesia.*
[3] *Earthquake Research Group, National Research and Innovation Agency (BRIN), Bandung 40135, Indonesia.*
[4] *Indonesia Agency for Meteorology, Climatology and Geophysics (BMKG), Jakarta 10720, Indonesia.*
[5] *Department of Geophysical Engineering, Institut Teknologi Sepuluh Nopember, Surabaya, Indonesia.*
[6] *Research Center for Geological Disaster, National Research and Innovation Agency (BRIN), Bandung 40135, Indonesia.*

Abstract

The Palu–koro and Matano faults form a major bent strike-slip fault system in central Sulawesi, Indonesia, accommodating significant crustal deformation associated with regional plate interactions. In this study, we investigate the mechanical response of this fault system using three-dimensional numerical modelling to evaluate how different lateral loading configurations influence fault slip and stress patterns. Dirichlet (displacement-rate) boundary conditions, inferred from regional plate velocities, are applied to the model domain at the x-face, y-face, and in combined x- and y-face configurations. Models with pure x-face or y-face loading generate lateral slip patterns that are mechanically compatible with idealized Riedel shear kinematics; however, the resulting slip sense differs from the present day tectonic motion of the Palu–koro and Matano faults. In contrast, models with combined boundary conditions reproduce first-order characteristics of the observed fault behaviour. In particular, scenarios with dominant lateral loading at the x-face (e.g. 70% x-face and 30% y-face) produce predominantly sinistral slip along both faults and higher slip concentrations along the Palu–koro Fault, consistent with tectonic and geodetic observations. The combined loading models also exhibit a subtle rotation of the maximum principal stress orientation from WNW–ESE along the Palu–koro Fault to NE–SW along the Matano Fault, which is qualitatively consistent with stress orientations inferred from focal mechanism inversions. Overall, the results suggest that combined regional lateral loading, with a dominant north–south lateral movement, provides a plausible mechanical framework for understanding deformation localization and stress rotation within the Palu–koro–Matano fault system.

Keywords:
bent strike-slip; fault lateral slip; fault tensile slip; Matano Fault; numerical modelling; Palu-koro Fault; Riedel shear

1. Introduction

Several conceptual models have been developed by structural geologists to explain rock deformation. One such model is the simple shear model, in which parallel planes slide past one another laterally, transforming an initially square material element into a rhombus (**Harding, 1973**). This parallel lateral loading causes the material to undergo both shear and rotation, such that one diagonal experiences shortening while the other undergoes extension. The maximum principal stress axis is aligned with the compressional (shortening) diagonal, whereas the minimum principal stress axis is aligned with the extensional diagonal (**Davis and Reynolds, 1996**; **Ragan, 1973**). Within such a simple shear system, internal faulting patterns known as Riedel structures develop, consisting of synthetic and antithetic strike-slip shear fractures (**Kavyani-Sadr et al., 2022**; **Riedel, 1929**) (see **Figure 1**).

The Palu-koro and Matano faults are located on the island of Sulawesi in eastern Indonesia, where the tectonic setting is complex due to the collision of four plates: the Eurasian/ Sunda, Australian, Philippine sea, and Pacific plates (**Hall, 2012**; **Hamilton, 1979**; **Silver et al., 1983**) (see **Figure 2**). The Australian Plate moves north-northeastwardly, while the Philippine Sea and Pacific plates move northwestwardly relative to the Eurasian/Sunda Plate (**DeMets et al., 2010**), generating both north–south and east–west components of regional lateral tectonic loading.

* Corresponding author: Nanang T. Puspito
e-mail address: nanangpuspito@gmail.com
Received: 18 September 2025. Accepted: 26 January 2026.
Available online: 21 July 2026

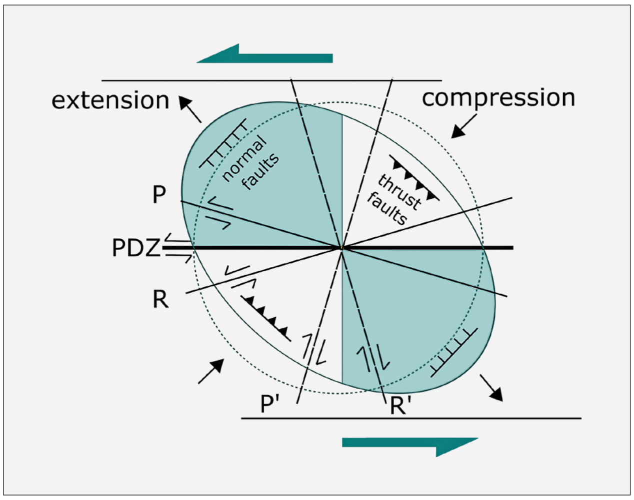

Figure 1: Schematic diagram of a sinistral Riedel shear zone developed under simple shear deformation. PDZ denotes the principal displacement zone. R represents the Riedel shear and P represents the synthetic secondary shear. R' and P' are the conjugate Riedel shear and the conjugate secondary shear, both exhibiting antithetic motion relative to the PDZ. The green shaded areas indicate tensile quadrants, whereas the white areas represent compressional quadrants. The dashed circle is the undeformed model. Modified after **Riedel (1929)**, **Yu et al. (2022)**, and **Roy et al. (2021)**.

Stress inversion has been used to study the deformation of Sulawesi. **Beaudouin et al. (2003)** divided the island of Sulawesi into several zones and performed stress inversion using focal mechanism data to obtain σ_H orientations. They observed areas of contraction and extension in Sulawesi. In the following studies, stress orientation in the Palu-koro and Matano faults, have been inverted using focal mechanism data. Northwest-southeast (NW-SE) stress orientation in the Palu-koro Fault and northeast-southwest (NE-SW) stress orientation in the Matano Fault are observed (**Kusumawati et al. 2025**; **Octhav et al., 2025**) (see **Figure 2**). These rotating stress orientations provide important evidence for evaluating the mechanical response of bent strike-slip faults to regional lateral tectonic loading.

Numerical modelling is common for studying geodynamics, where direct observation is limited. It can be used to study the dynamics of the Earth by solving and simulating the physical processes (**Gerya, 2019**; **Zelst et al., 2021**). Several studies have applied numerical modelling and explained the deformation surrounding the faults. **Wang et al. (2017)** applied numerical modelling to simple stepovers and bends using a 3-D finite element code to study the stress perturbation, strain partitioning, and fault evolution. Their model predicts the stress and strain distribution around stepovers and bends, and explains the key differences between these configurations in the Dead Sea trough, Death Valley, and along the San Andreas Fault. **Bening et al. (2022)** study the fault deformation during strain buildup and release in a strike-slip fault with a brittle elastic-viscoelastic material. The modelling results explained the pattern of seismicity observed on the Great Sumatran Fault.

Utilizing numerical modelling to analyze continuum crustal deformation, we investigate how regional lateral loading, represented by a simple shear framework, influences deformation within a bent strike-slip fault system. The Palu–koro and Matano faults, subjected to regional tectonic loading from both east-west and north-south directions, serve as natural examples for our analysis. The rotating stress orientations observed along these faults serve as qualitative reference patterns for exploring the mechanical response of bent strike-slip systems to lateral loading. Accordingly, we apply several lateral loading scenarios to examine deformation localization at the faults, as expressed by fault slip distributions, and the resulting stress orientation. We then further compared them to the present-day conditions of the faults. The results indicate that combined lateral loading, dominated by a north–south direction, provides the consistent explanation for observed fault slip distributions and stress orientations, offering a mechanical explanation for the higher slip rate and shorter recurrence behaviour of the Palu–koro Fault relative to the Matano Fault.

2. Tectonic setting

The Palu–koro and Matano faults in Indonesia are located within the Sunda Plate, at the western termination of a major sinistral strike-slip fault system in eastern Indonesia that extends from Papua to Sulawesi. The major sinistral strike-slip fault system consist of the Yapen and Sorong faults in Papua, the Sula–Sorong fault zone in North Molucca, the Matano and Palu-koro faults in Sulawesi, that further terminates at the Sulawesi subduction trench in the north (**Silver et al., 1983**; **Hamilton, 1979**) (see **Figure 2**). The sinistral strike-slip fault system developed in response to the oblique convergence of the Australian, Philippine Sea, and Pacific plates relative to the Eurasian/Sunda Plate (**Hall, 2012**; **Hamilton, 1979**; **Silver et al., 1983**). The Australian Plate moves north-northeastward at a rate of 76 mm/year, whereas the Philippine Sea and Pacific plates move northwestward at rates of 106 mm/year and 101 mm/year (**DeMets et al., 2010**), respectively. The complex plate interaction strongly influences the kinematics of the Palu–koro and Matano faults, as demonstrated by microblock rotation model that explain the observed geodetic velocity field in Sulawesi (**Socquet et al., 2006**).

The development of the Palu–koro and Matano faults consisted of two main periods of tectonic activity: (1) the Mesozoic–Paleogene and (2) the Neogene (**Baillie and Decker, 2022**; **Hall and Wilson, 2000**). During the Mesozoic–Paleogene, the main tectonic blocks that later formed Sulawesi were formed (**Hall, 2012**). In the Neogene, these blocks moved, rotated, and interacted through complex geological processes, leading to the development of the present day K-shaped Sulawesi

(**Hall and Wilson, 2000**; **Socquet et al., 2006**). Within this framework, the Palu–koro and Matano faults developed in association with the present configuration of the tectonic blocks, while the oblique convergence at the regional scale may have contributed to the observed left-lateral slip motion along the faults.

3. Methodology

3.1. Data

In this study, we formed a block model of the Palu-koro and Matano faults to run the numerical modelling. The block was built with a size of 3.5º length and 3.75º width over the area of central Sulawesi, with the Palu-koro and Matano faults located at the center of the block. We created an elastic half-space model for the block with 80 km thickness of elastic layer to simplify the model. For the depth of the fault, we set it from 0 to 30 km depth, considering the average Moho discontinuity depth in Sulawesi from CRUST1.0 (**Laske et al., 2013**). The material properties were also referred from CRUST1.0: the density, P- and S-wave velocity of 2780 kg/m^3, 6385 m/s, and 3663 m/s for 0 to 30 km depth; and 3113 kg/m^3, 7437 m/s, and 4177.3 m/s for 30 to 50 km depth, respectively.

We considered ten segments of the Palu-koro and Matano faults in the model: Donggala, Palu, Saluki, Moa, Meloi, Kuleana, Pewusai, Matano, Pamsoa, and Ballawai segments. The segments were referred from the National Center for Earthquake Studies of Indonesia **(PUSGEN) (2017)**, **Natawidjaja et al. (2021)**, and **Daryono (2016)**, as shown in **Figure 2**. The observation target is the regional deformations of the faults, thus we modelled a simplified version of the faults by excluding the fault details in some segments, such as the fault's branching in the Palu segment and the fault stepover in Matano Lake. We modelled these parts as continuous segments.

The block is divided into a hexahedral mesh consisting of 6834 cells and 8304 nodes. Due to the non-planar geometry of the fault, the mesh size adapts to the curvature of the fault while maintaining the hexahedral shape of the cell. The size of the cells near the bend of the fault is smaller than the cells at the planar part of the fault. The maximum, minimum, and average cell edge lengths are 21.51 km, 6.44 km, and 12.71 km, respectively. The average size of the cell edge is still smaller than the length of the fault segment, 18.8 km to 66.5 km **(PUSGEN, 2017)**, thus still considered as a reliable resolution for the modelling. The mesh in this study was created using Coreform Cubit 2021.11 (Coreform, Orem, UT, USA). Coreform Cubit is software for creating high-quality finite element analysis meshes.

3.2. Method

We used the finite element method for the numerical modelling, implemented in Pylith software. Pylith is a finite element software for simulating dynamic and quasi-static deformation of the crust, including simulating the deformation due to fault slip (**Aagaard et al., 2017, 2013**). The software uses the domain decomposition approach in the fault slip implementation and the Krylov subspace method to solve the linear equation.

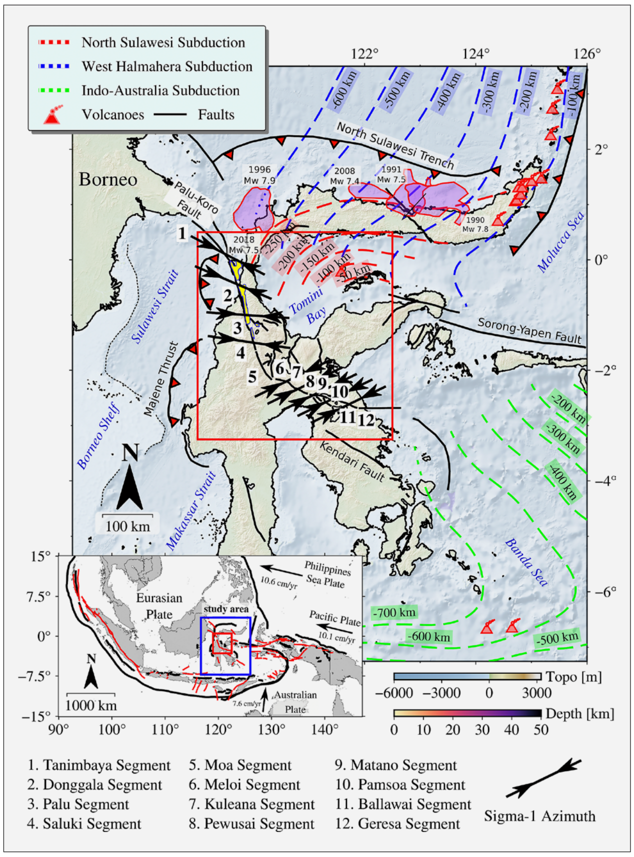

Figure 2: Tectonic setting of Sulawesi and surrounding regions. The historical earthquake slip models (purple) from **Zheng et al. (2023)** highlight major events ($M_w > 7$), including the 2018 M_w 7.5 Palu earthquake (yellow). The dashed lines denote major subduction systems: North Sulawesi (red), West Halmahera (blue), and Indo-Australian (green) (**Hayes et al., 2018**). Maximum principal stress (σ_1) azimuths along the Palu–koro and Matano faults are shown after **Kusumawati et al. (2025)** and **Octav et al. (2025)**. The red square outlines the numerical modelling domain. The bathymetry profile were downloaded from BATNAS-BIG (https://sibatnas.big.go.id/), fault line from **PUSGEN (2017)**, **Natawidjaja et al. (2021)**, and **Daryono (2016)**.

Based on the regional tectonic setting of Palu-koro and Matano faults, the oblique convergence of the Australian, Phillipine Sea, and Pacific plates relative to the Eurasian/Sunda Plate produces an average relative plate motion vector of 97 mm/year directed northwestward. This displacement rate magnitude was used to define three lateral loading scenarios, representing the regional tectonic loading. We imposed the lateral loading by prescribing Dirichlet (displacement) boundary conditions on the lateral faces of the model domain. The coordinate system was defined such that the east, north, and upward directions correspond to the positive x-, y-, and z-axes, respectively.

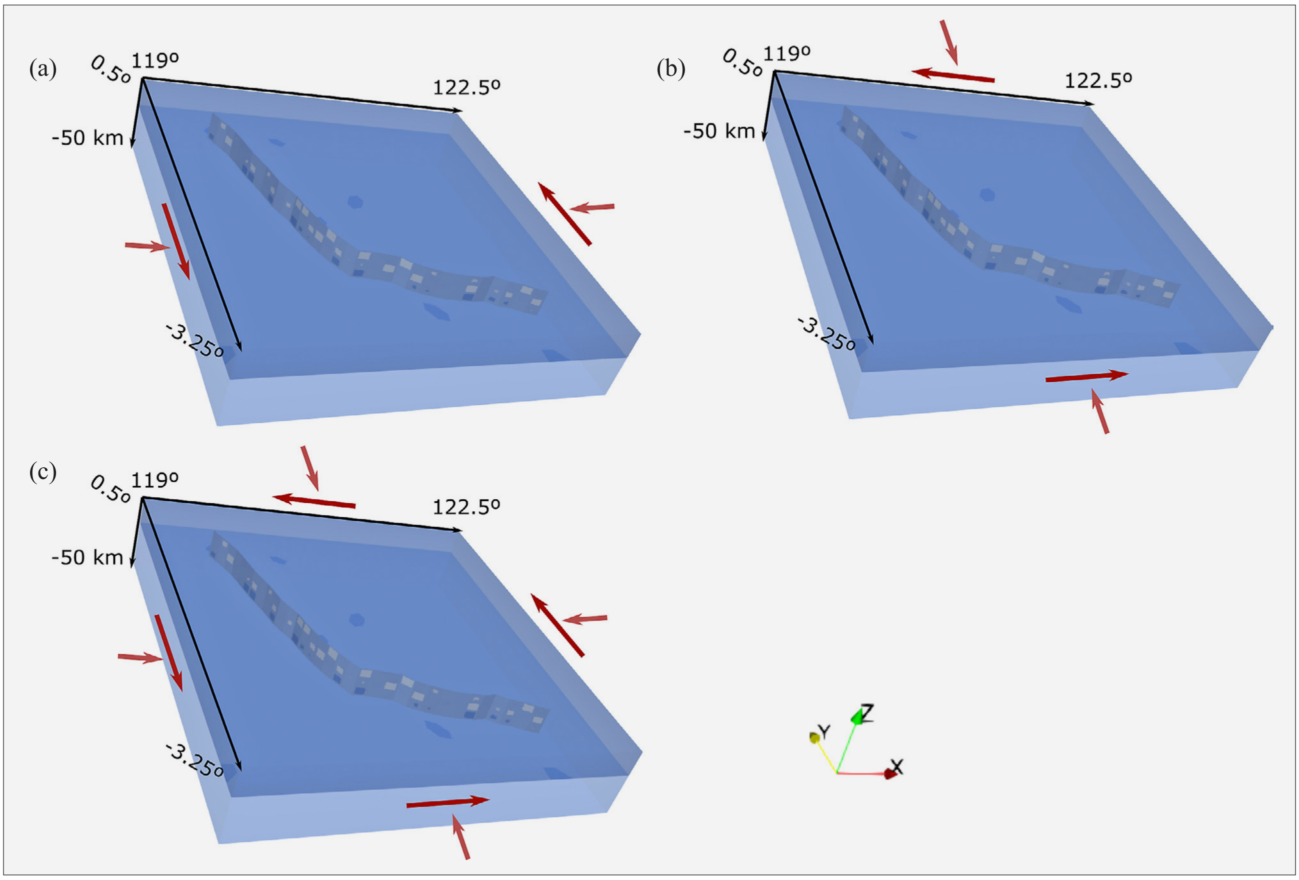

Figure 3: Model set up and boundary condition: (a) the x-face boundary condition, (b) the y-face boundary condition, (c) the combine x- and y-faces boundary conditions. The x- y- and z-axis are showing the east, north and up directions.

Tabel 1: Combine x- and y-faces boundary conditions, displacement rate magnitude propotion at the x- and y-faces: 10%:90%, 30%:70%, 50%:50%, 70%:30%, and 90%:10%.

Proportion (x- and y-faces) 10%:90%		
Faces	Disp. rate x (mm/year)	Disp. rate y (mm/year)
xpos	-5	10
xneg	5	-10
ypos	-87	-5
yneg	87	5

Proportion (x- and y-faces) 50%:50%		
Faces	Disp. rate x (mm/year)	Disp. rate y (mm/year)
xpos	-5	49
xneg	5	-49
ypos	-49	-5
yneg	49	5

Proportion (x- and y-faces) 90%:10%		
Faces	Disp. rate x (mm/year)	Disp. rate y (mm/year)
xpos	-5	87
xneg	5	-87
ypos	-10	-5
yneg	10	5

Proportion (x- and y-faces) 30%:70%		
Faces	Disp. rate x (mm/year)	Disp. rate y (mm/year)
xpos	-5	29
xneg	5	-29
ypos	-68	-5
yneg	68	5

Proportion (x- and y-faces) 70%:30%		
Faces	Disp. rate x (mm/year)	Disp. rate y (mm/year)
xpos	-5	68
xneg	5	-68
ypos	-29	-5
yneg	29	5

- The x-face boundary condition

  In the first scenario, we applied shear displacement rate of 97 mm/year on the x-faces of the model domain, as shown in **Figure 3a**, generating north-south lateral movement with a left lateral or sinistral sense of motion. An axial displacement of approximately 5% of the imposed shear rate (≈5 mm/year), was applied to the x-faces together with the shear displacement to maintain compresive normal traction on the fault (**Aagaard et al., 2017**). This configuration is hereafter referred to as the *x-face boundary condition*.

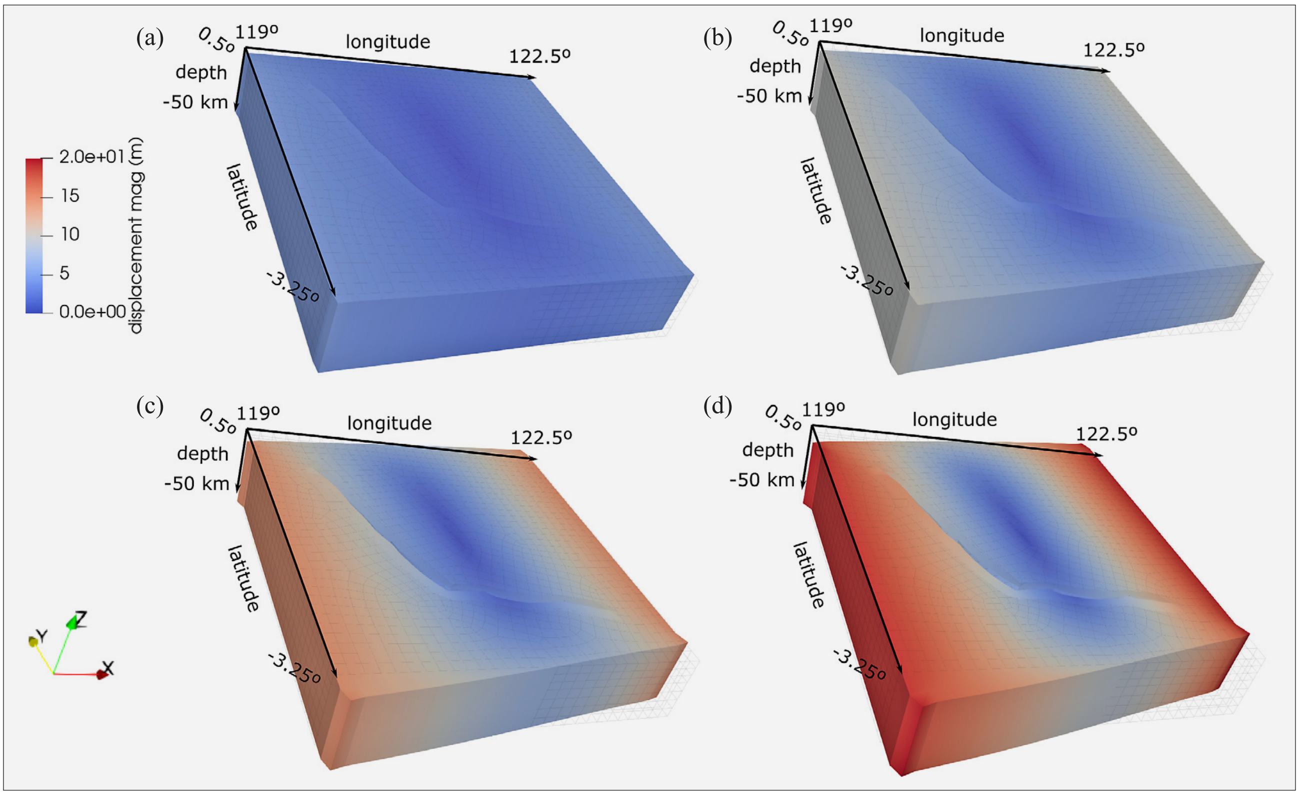

Figure 4: The displacement magnitude (m) of block deformation for the x-face boundary condition, at: (a) year 50, (b) year 100, (c) year 150, and (d) year 200. The figure is exagerated by a factor of 2000. The gray mesh is the original undeformed form of the block. The x- y- and z-axis are showing the east, north and up directions.

- The y-face boundary condition

  In the second scenario, we applied shear and axial displacement rates of 97 mm/year and ≈5 mm/year, at the y-faces of the model domain as shown in **Figure 3b**. The boundary condition creates west-east lateral movement on the y-faces with a left lateral or sinistral sense of motion. This configuration is hereafter referred to as the *y-face boundary condition*.
- The combine x- and y-faces boundary conditions

  We combined the x-face and y-face boundary conditions for the third scenario, to approximate natural tectonic loading involving both north–south and west-east components. The relative contribution of shear displacement rate applied to the x- and y-faces was varied in proportions of 10%:90%, 30%:70%, 50%:50%, 70%:30%, and 90%:10%, respectively (**Figure 3c**; **Table 1**). The axial displacement rate was kept constant across all combined-loading cases. This configuration is hereafter referred to as the *combine x- and y-faces boundary conditions.*

The load due to displacement at the boundary condition will generate shear and normal stresses on the fault surface. A slip on the fault will occur when the stresses overcome the fault constitutive model. In this study, fault behaviour is governed by static friction constitutive law, in which the fault will slip when the shear stress (τ) is equal to or greater than the failure resistance component. The failure resistance consists of fault cohesive strength (C) and fault static friction (μ_s) multiplied by the effective normal stress (σ'), which is the normal stress subtracted by fluid pore pressure (**Oppenheimer et al., 1988**; **Sibson, 1974**), following the Coulomb failure criterion (**Equation 1**).

$$\tau = C + \mu_s \sigma' \tag{1}$$

A cohesion value of 0 MPa was assigned to account for the pre-existing fault with neglible cohesive strenght. A static friction of 0.5 was adopted, corresponding to a moderately strong fault and lying slightly below the lower bound of Byerlee friction ($0.6 < \mu_s < 0.8$) (**Collettini et al., 2019**). A simulation was perfomed over a duration of 200 years. Since the objective of this study is to investigate the mechanical response of bent strike-slip faults to regional lateral tectonic loading – rather than the coseismic processes – the use of a static friction formulation within an elastic half-space framework is sufficient and computationally efficient. Model results were visualized using Paraview (**Ahrens et al., 2014, 2005**).

The imposed boundary conditions produce a deformation of the model block, expressed as displacement magnitudes (m) in the x-, y-, and z-directions at mesh nodes. These boundary conditions also drive fault motion, quantified in terms of fault slip (m), including both lateral and tensile slips components. In addition, the applied loading generates stresses throughout the model

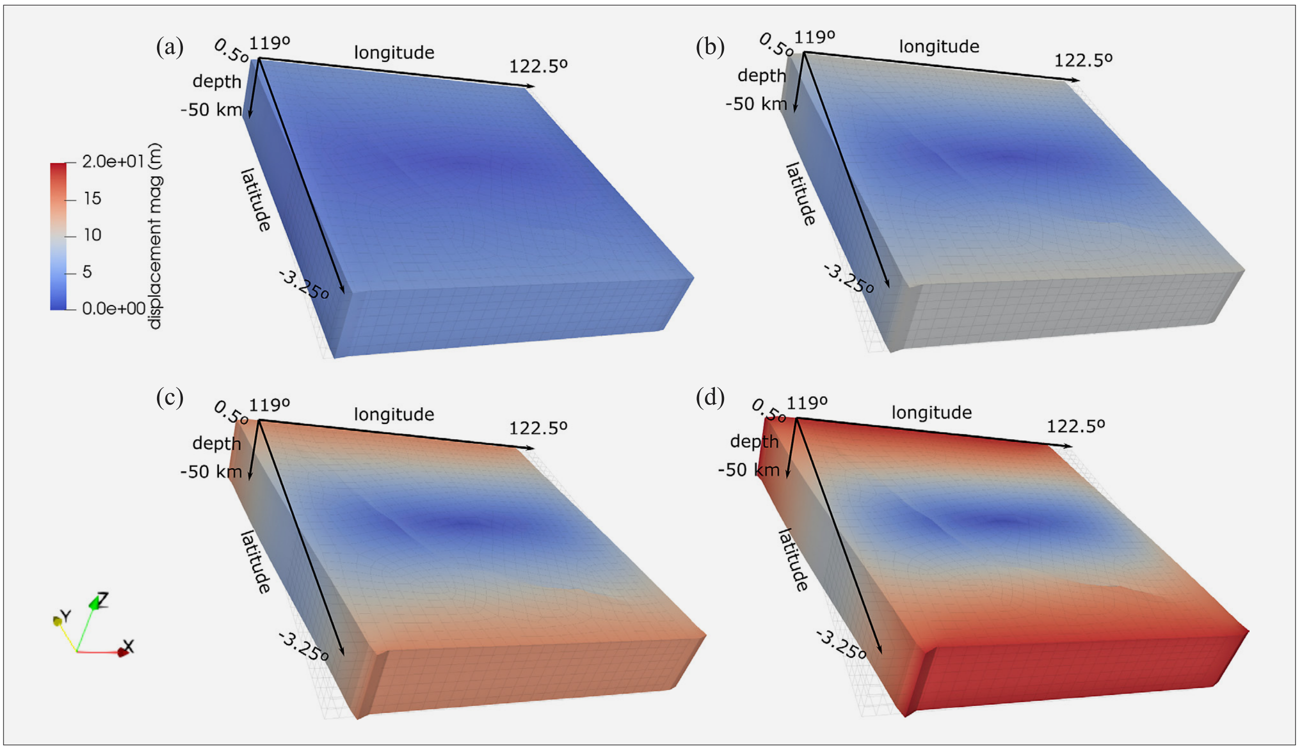

Figure 5: The displacement magnitude (m) of block deformation for the y-face boundary condition, at: (a) year 50, (b) year 100, (c) year 150, and (d) year 200. The figure is exagerated by a factor of 2000. The gray mesh is the original undeformed form of the block. The x- y- and z-axis are showing the east, north and up directions.

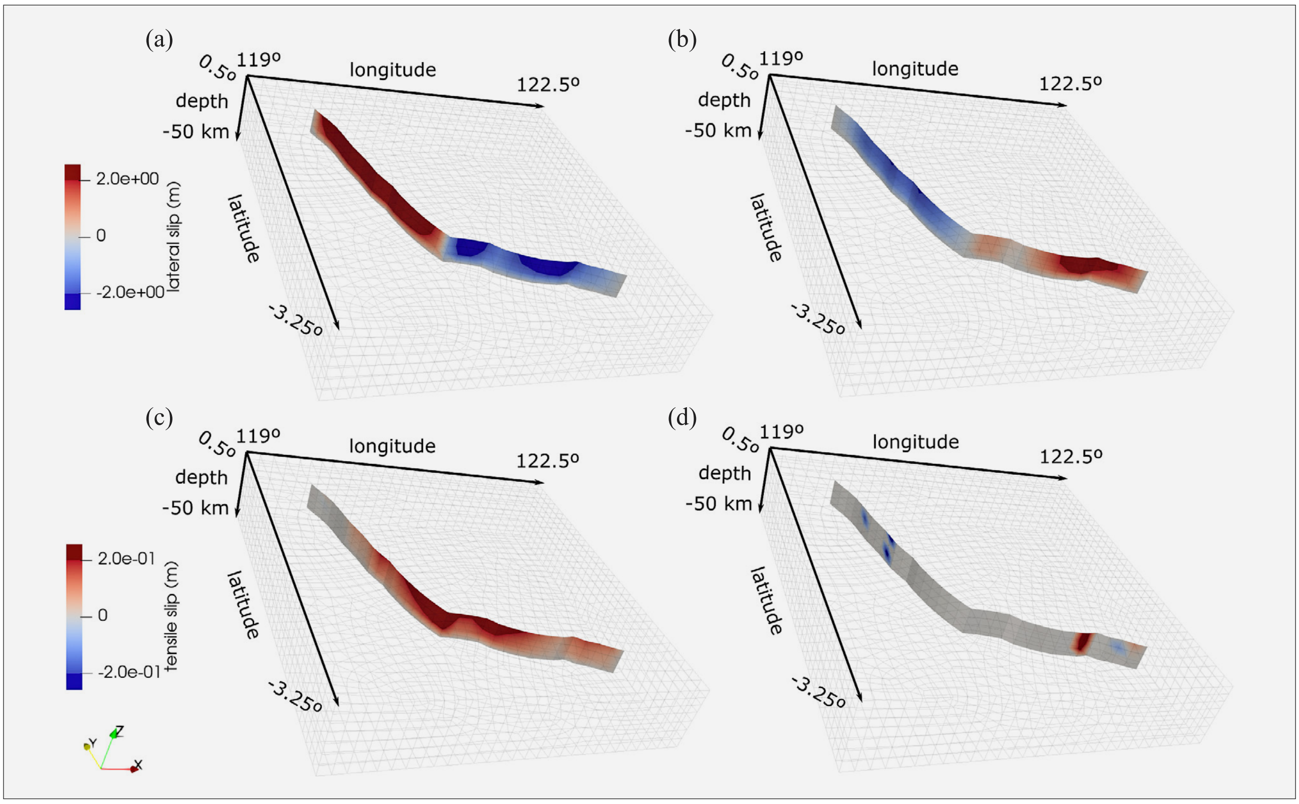

Figure 6: The fault slip, represented by the lateral and tensile slip (m), on the Palu-koro and Matano faults at year 200 for: (a) the x-face boundary condition lateral slip (m), (b) the y-face boundary condition lateral slip (m), (c) the x-face boundary condition tensile slip (m), (d) the y-face boundary condition tensile slip (m). The gray mesh is the original undeformed form of the block. The x- y- and z-axis are showing the east, north and up directions. Positive lateral slip represents a left lateral motion, while positive tensile slip represents an opening.

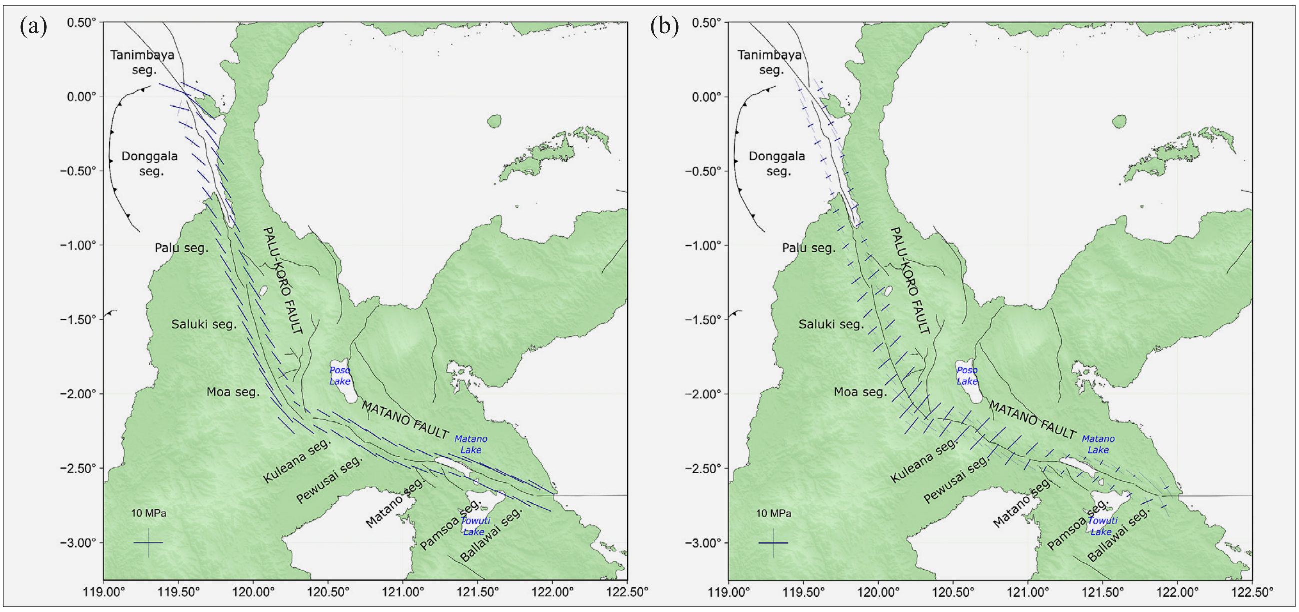

Figure 7: Maximum principal stress (bold dark blue line) along the Palu-koro and Matano faults for: (a) the x-face boundary condition, (b) the y-face boundary condition. The principal stress was estimated from the deformation at year 200.

domain, represented by the stress tensor computed at mesh cells. From the stress tensor, we estimated the principal stress magnitudes and azimuths to characterize the resulting stress orientation within the model.

4. Results

4.1. The x-face boundary condition

As the simulation time increases from 50 to 200 years, the displacement magnitude in the x-face boundary condition model progressively increases from the positive and negative x-boundaries toward the center of the domain, producing a vertically oriented zone of relatively low displacement at the model center (see **Figure 4**). The resulting fault slip pattern shows positive lateral slip (left-lateral motion) up to 2 m, along the Palu–koro Fault and negative lateral slip (right-lateral motion) along the Matano Fault (see **Figure 6a**). The left-lateral slip along the Palu–koro Fault is interpreted to result from its orientation, which is nearly parallel to the imposed x-face boundary loading. Under this configuration, the Palu–koro Fault accommodates shear in the same sense as the applied lateral motion, analogous to a Riedel shear (R) motion in a simple-shear system. In contrast, the Matano Fault trends WNW–ESE and is oriented nearly perpendicular to the x-face boundary, resulting in antithetic motion relative to the imposed shear, and this behaviour is consistent with the kinematics of a conjugate secondary shear (P’) within a simple-shear framework (see **Figure 1**).

Positive tensile slip (fault opening) is observed from the southern segment of the Palu–koro Fault, near the bending, toward the Matano Fault (see **Figure 6c**). In particular, the opening is highly concentrated near the fault bend and along the western segment of the Matano Fault, which is interpreted to result from the combined effects of fault geometry and the WNW–ESE orientation of the Matano Fault relative to the imposed lateral loading. The estimated maximum principal stress direction shows a broadly uniform northwest–southeast orientation from the Palu–Koro Fault to the Matano Fault (see **Figure 7a**). This stress pattern is likely influenced by the imposed north–south lateral movement at the x-face boundary condition and is broadly consistent with the orientation of the compressional axis expected under simple-shear deformation.

4.2. The y-face boundary condition

In the y-face boundary-condition model, the displacement magnitude is highest, up to 20 m, along the y-faces and gradually decreases toward the center of the domain, forming a zone of relatively low displacement with an orientation parallel to the y-faces (see **Figure 5**). The resulting fault-slip pattern differs from that observed in the x-face boundary condition scenario. Positive lateral slip (left-lateral motion) is concentrated along the Matano Fault, whereas negative lateral slip (right-lateral motion) occurs along the Palu–Koro Fault (see **Figure 6b**). The left-lateral slip along the Matano Fault is compatible with the kinematics of a synthetic secondary shear (P) that accommodates deformation in the same sense as the imposed lateral motion. In contrast, the right-lateral slip along the Palu–Koro Fault is consistent with the behaviour of a conjugate Riedel shear (R′), exhibiting antithetic motion relative to the applied lateral loading (see **Figure 1**).

Tensile slip in the y-face boundary-condition model exhibits fewer and more limited opening areas compared to the x-face boundary condition scenario. Localized

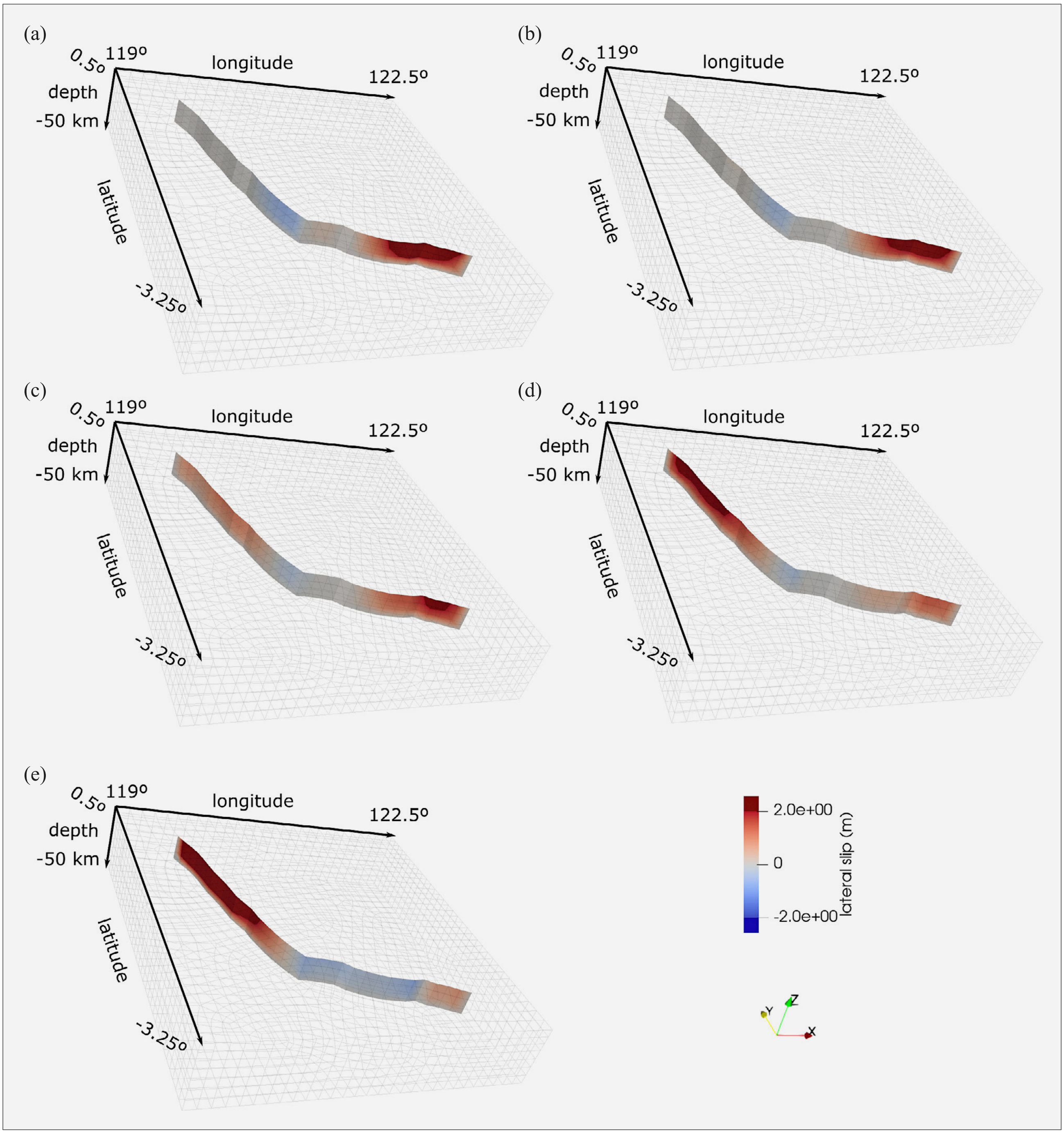

Figure 8: The fault slip, represented by the lateral slip (m), on the Palu-koro and Matano faults at year 200 for the combined x- and y-faces boundary conditions, with x- and y-faces percentage proportion: (a) 10%:90%, (b) 30%:70%, (c) 50%:50%, (d) 70%:30%, (e) 90%:10%, The x- y- and z-axis are showing the east, north and up directions. Positive lateral slip represents a left lateral motion.

positive tensile slip (opening) is mainly observed along the eastern segment of the Matano Fault, which may be related to local fault geometry (see **Figure 6d**). The maximum principal stress orientation in the y-face boundary-condition model shows a relatively uniform northeast–southwest trend (see **Figure 7b**). This stress orientation is largely perpendicular to the fault strike, which may contribute to the generally limited development of opening along the fault.

4.3. The combine x- and y-faces boundary conditions

The modelling results for the combined x- and y-face boundary-condition scenarios are illustrated by the lateral slip (see **Figure 8**) and tensile slip (see **Figure 9**). For scenarios with a small displacement-rate contribution on the x-faces (see **Figure 8a)**, the fault slip pattern closely resembles that of the y-face boundary condition model, with

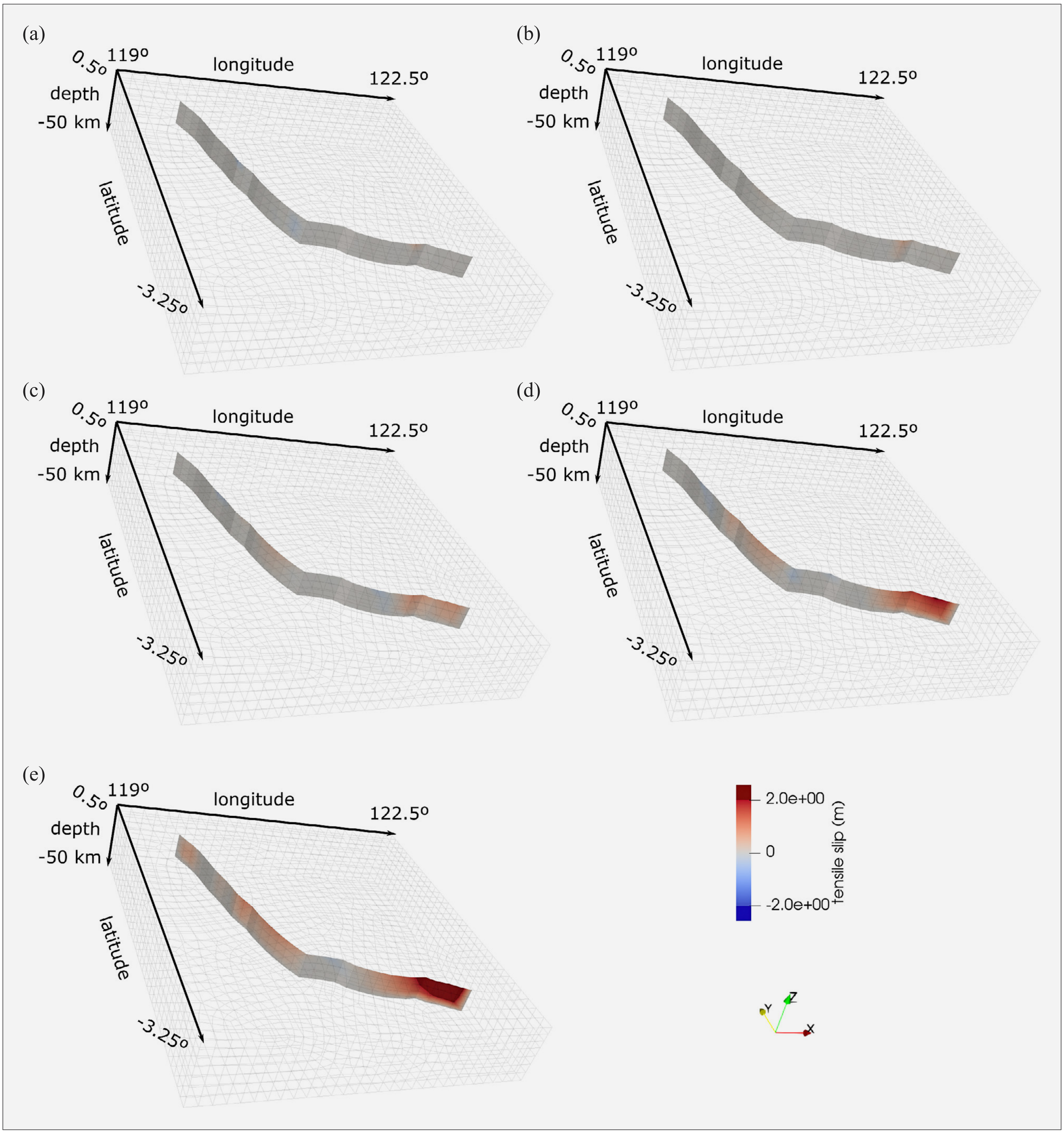

Figure 9: The fault slip, represented by the tensile slip (m), on the Palu-koro and Matano faults at year 200 for the combined x- and y-faces boundary conditions, with x- and y-faces percentage proportion: (a) 10%:90%, (b) 30%:70%, (c) 50%:50%, (d) 70%:30%, (e) 90%:10%, The x- y- and z-axis are showing the east, north and up directions. Positive tensile slip represents an opening.

positive lateral slip concentrated along the Matano Fault. In contrast, scenarios with a large displacement rate contribution on the x-faces (see **Figure 8e**) produce slip distributions similar to those of the x-face boundary condition scenario, with dominant positive slip along the Palu–koro Fault. In general, as the proportion of displacement applied on the x-faces increases from 10% to 90%, the magnitude of positive lateral slip along the Matano Fault progressively decreases, while slip becomes increasingly distributed along the Palu–koro Fault (see **Figure 8a–e**). For the tensile slip, positive tensile slip (opening) is distributed at the Matano Fault as the proportion of displacement rate increases on the x-faces (see **Figure 9a-e**). However, the concentration of the opening is located at the easternmost part fo the Matano Fault, in contrast with the x-face boundary condition scenario (see **Figure 6c**).

In general, the maximum principal stress orientations produced by the combined boundary condition models

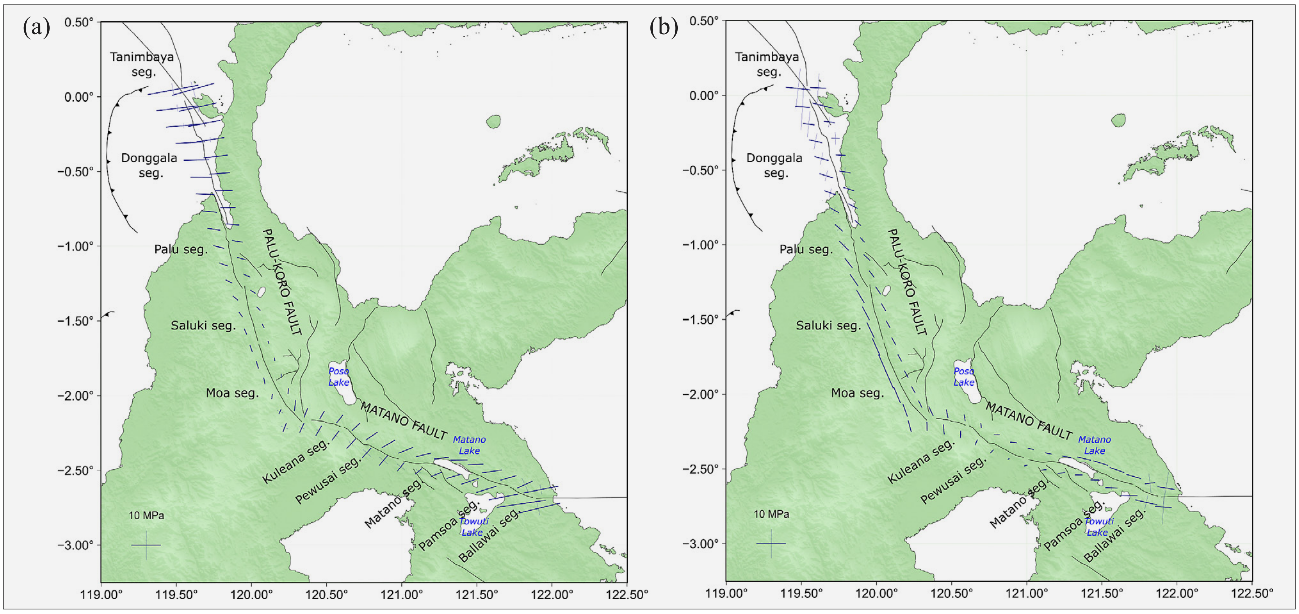

Figure 10: Maximum principal stress (bold dark blue line) along the Palu-koro and Matano faults for the combined x- and y-faces boundary conditions, with x- and y-faces percentage: (a) 30%:70%, (b) 70%:30%. The principal stress was estimated from the deformation at year 200.

exhibit spatially non-uniform azimuths, with its orientation influence by the dominant displacement rate component. Representative results are shown for the 30%:70% (x-face 30%) scenario (see **Figure 10a**) and the 70%:30% (x-face 70%) scenario (see **Figure 10b**). For the x-face 30% scenario, the maximum principal stress along the Palu–koro Fault is oriented predominantly E–W to WNW–ESE. In contrast, the x-face 70% scenario yields a stress orientation along the Palu–koro Fault that is rotated toward a more NW–SE trend. Along the Matano Fault, the maximum principal stress shows a consistent NE–SW orientation throughout the fault for the x-face 30% scenario. For the x-face 70% scenario, a NE–SW orientation is maintained primarily between Lake Matano and Lake Towuti, while stress orientations outside this area become more parallel with the fault strike.

5. Discussion

The fault-slip motions produced by the pure x-face and y-face boundary-condition models are mechanically consistent with the classical Riedel shear system (see **Figure 6**), suggesting that Riedel shear kinematics may be applicable to bent strike-slip systems for describing idealized slip patterns. However, this consistency does not imply that the Palu–Koro and Matano faults formed as Riedel fractures generated by simple shear deformation.

In comparison with the present-day tectonic behaviour of the Palu–koro and Matano faults, the pure x-face and y-face boundary-condition models do not adequately reproduce the observed fault motions. Observations indicate that both faults accommodate predominantly sinistral motion, driven by the westward motion of the Philippine Sea and Pacific plates relative to the Eurasian/Sunda Plate, within which Sulawesi is located. Geodetic velocity measurements in the Palu–koro region reveal a rotation of velocity vectors from NW–SE to NNW–SSE, which has been successfully explained by microblock rotation models (**Socquet et al., 2006**). This rotation facilitates the transfer and continuity of left-lateral motion from the Matano Fault to the Palu–koro Fault.

Among the modelled scenarios, the combined x-face and y-face boundary conditions with a dominant x-face rate – particularly the x-face 70% configuration – most closely reproduce this tectonic behaviour. This scenario yields sinistral slip along both the Palu–koro and Matano faults, with a higher concentration of slip localized on the Palu–koro Fault (see **Figure 8d**). The high concentration slip at the Palu-koro Fault, is consistent with reported geodetic and geological estimates indicating a higher fault slip rate along the Palu–koro (≈35-40 mm/year) compared to the Matano Fault (≈20-21 mm/ year) (**Bellier et al., 2001**; **Patria et al., 2023**; **Socquet et al., 2006**). The dominance of north–south lateral loading in the preferred configuration of this study is also broadly compatible with northward microblock rotation inferred from geodetic observations (**Socquet et al., 2006**).

Although subtle, rotation of the maximum principal stress orientation is observed in the combined x-face and y-face boundary condition models (see **Figure 10**). In the x-face 30% configuration, the maximum principal stress orientation transitions from WNW–ESE along the Palu–koro Fault to NE–SW along the Matano Fault. A similar spatial variation is observed in the x-face 70% configuration, with orientations changing from NW–SE at the Palu–koro Fault to NE–SW at the Matano Fault. This pattern likely reflects the superposition of lateral loading applied at the x-face and y-face boundaries, where x-face loading favors NW–SE–oriented stresses and y-face loading favors NE–SW–oriented stresses (see **Figure 7**).

In general, the numerical models with combined boundary condition configurations with a dominant north–south lateral loading applied at the x-face, reproduce fault slip distributions that are broadly consistent with the present day kinematics of the Palu–koro and Matano faults. The modelled sinistral motion, higher slip concentration along the Palu–koro Fault, and rotation in stress orientation are qualitatively compatible with geological and geodetic observations. However, the imposed proportions of north–south and east–west lateral loading at the x-face and y-face represent simplified approximations of the regional tectonic loading. Future studies should consider observed geodetic velocity fields in Sulawesi to better constrain boundary condition rates and improve the numerical modelling results.

6. Conclusions

We investigated the mechanical response of a bent strike-slip fault system, represented by the Palu–koro and Matano faults, using numerical modelling with Dirichlet (displacement rate) boundary conditions applied at the x-face, y-face, and combined x- and y-faces of the model domain, with rate value infered from the regional plate velocity. The conclusions are described as follows.

1. Models with pure x-face or y-face loading produce lateral slip patterns that are compatible with idealized Riedel shear kinematics; however, these patterns differ from the present-day tectonic motion of the fault system.
2. Combined boundary condition models reproduce first-order characteristics of the observed fault behaviour, including spatial variations in stress orientation along the Palu–koro and Matano faults.
3. Particularly, the model with a dominant lateral loading at the x-face, e.g. 70% x-face and 30% y-face (dominantly north–south lateral movement) produces a predominantly sinistral slip along both faults and a higher slip concentration along the Palu–koro Fault, consistent with tectonic observations.
4. A rotation in maximum principal stress orientation from WNW–ESE along the Palu–koro Fault to NE–SW along the Matano Fault is also observed, which is qualitatively consistent with stress orientations inferred from focal mechanism inversions.

The combined regional lateral loading with a dominant north–south component provides a plausible mechanical framework for understanding deformation localization and stress rotation within the Palu–Koro–Matano fault system. Although this study does not explicitly address long-term geodynamic evolution, the results offer mechanical insight into how present-day regional lateral loading interacts with the existing Palu-Koro-Matano fault geometry and caused the slip accumulation as well as stress rotation along the faults.

7. Nomenclature

Symbol/ term	Description
xpos	boundary condition plane at x = 122.5º
xneg	boundary condition plane at x = 119º
ypos	boundary condition plane at x = 0.5º
yneg	boundary condition plane at y = -3.25º
x-face	xpos and xneg boundary condition
y-face	ypos and yneg boundary condition
x-face 30%	boundary condition with proportion 30% of shear displacement rate applied at the x-face and 70% of shear displacement rate applied at the y-face
x-face 70%	boundary condition with proportion 70% of shear displacement rate applied at the x-face and 30% of shear displacement rate applied at the y-face

Acknowledgement

The figures were generated with Generic Mapping Tools in Python (PyGMT) (**Uieda and Wessel, 2017**) and Paraview (**Ahrens et al., 2014, 2005**).

Funding

This research was funded by the Indonesia Ministry of Education, Culture, Research, and Technology (Direktorat Riset, Teknologi, dan Pengabdian kepada Masyarakat (DRTPM) Direktorat Jenderal Pendidikan Tinggi, Riset, dan Teknologi (Ditjen Diktiristek) Kementerian Pendidikan, Kebudayaan, Riset, dan Teknologi (Kemendikbudristek) Republik Indonesia), grant number 303/IT1.B07.1/SPP-LPPM/VI/2024. The research fund was under the research scheme of the Doctoral Dissertation Postgraduate Research Program granted to NTP as the promotor and DK as the doctoral student in 2024, with the research title “Pemodelan numerik 3D sesar gesar sintetik dan riil: studi kasus sesar Palu-koro dan Matano, Sulawesi, dan korelasi dengan kegempaan observasi”

8. References

Aagaard, B., Knepley, M., & Williams, C. (2017). PyLith v2.2.0. https://doi.org/10.5281/zenodo.438705

Aagaard, B.T., Knepley, M.G., & Williams, C.A. (2013). A domain decomposition approach to implementing fault slip in finite-element models of quasi-static and dynamic crustal deformation. Journal of Geophysical Research:

Solid Earth 118, 3059–3079. https://doi.org/10.1002/jgrb.50217

Ahrens, J., Geveci, B., & Law, C. (2005). ParaView: An End-User Tool for Large-Data Visualization, in: Visualization Handbook. Elsevier, pp. 717–731. https://doi.org/10.1016/B978-012387582-2/50038-1

Ahrens, J., Jourdain, S., O'Leary, P., Patchett, J., Rogers, D.H., & Petersen, M. (2014). An Image-Based Approach to Extreme Scale in Situ Visualization and Analysis, in: SC '14: Proceedings of the International Conference for High Performance Computing, Networking, Storage and Analysis. Presented at the SC '14: the International Conference for High Performance Computing, Networking, Storage and Analysis, pp. 424–434. https://doi.org/10.1109/SC.2014.40

Baillie, P., & Decker, J. (2022). Enigmatic Sulawesi: The tectonic collage. Berita Sedimentologi 48, 1–30. https://doi.org/10.51835/bsed.2022.48.1.388

Beaudouin, T., Bellier, O., & Sébrier, M. (2003). Present-day stress and deformation fields within the Sulawesi Island area (Indonesia) : Geodynamic implications. Bulletin de la Societe Geologique de France 174, 305–317.

Bellier, O., Sébrier, M., Beaudouin, T., Villeneuve, M., Braucher, R., Bourlès, D., Siame, L., Putranto, E., & Pratomo, I. (2001). High slip rate for a low seismicity along the Palu-Koro active fault in central Sulawesi (Indonesia). Terra Nova 13, 463–470. https://doi.org/10.1046/j.1365-3121.2001.00382.x

Bening, M.A., Sahara, D.P., Triyoso, W., & Kusumawati, D. (2022). Modeling the Impact of the Viscoelastic Layer Thickness and the Frictional Strength to the Lithosphere Deformation in a Strike-Slip Fault: Insight to the Seismicity Pattern along the Great Sumatran Fault. GeoHazards 3, 452–464. https://doi.org/10.3390/geohazards3040023

Collettini, C., Tesei, T., Scuderi, M.M., Carpenter, B.M., & Viti, C. (2019). Beyond Byerlee friction, weak faults and implications for slip behavior. Earth and Planetary Science Letters 519, 245–263. https://doi.org/10.1016/j.epsl.2019.05.011

Daryono, M. R. (2016). Paleoseismology of Tropical Indonesia (Cases study in Sumatran Fault, Palukoro-Matano Fault, and Lembang Fault) (Paleoseismologi Tropis Indonesia (Dengan Studi Kasus di Sesar Sumatra, Sesar Palukoro-Matano, dan Sesar Lembang)). Dissertation Doctoral Program, Institut Teknologi Bandung (in Indonesian with English abstract)

Davis, G., & Reynolds, S. (1996). Structural Geology of Rocks and Regions, 2nd Edition.

DeMets, C., Gordon, R.G., & Argus, D.F. (2010). Geologically current plate motions. Geophysical Journal International 181, 1–80. https://doi.org/10.1111/j.1365-246X.2009.04491.x

Gerya, T. (2019). Introduction to Numerical Geodynamic Modelling, 2nd ed. Cambridge University Press, Cambridge. https://doi.org/10.1017/9781316534243

Hall, R. (2012). Late Jurassic–Cenozoic reconstructions of the Indonesian region and the Indian Ocean. Tectonophysics 570–571, 1–41. https://doi.org/10.1016/j.tecto.2012.04.021

Hall, R., & Wilson, M.E.J. (2000). Neogene sutures in eastern Indonesia. Journal of Asian Earth Sciences 18, 781–808. https://doi.org/10.1016/S1367-9120(00)00040-7

Hamilton, W.B. (1979). Tectonics of the Indonesian region (No. 1078), Professional Paper. U.S. Govt. Print. Off.,. https://doi.org/10.3133/pp1078

Harding, T.P. (1973). Newport-Inglewood Trend, California – An Example of Wrenching Style of Deformation1. AAPG Bulletin 57, 97–116. https://doi.org/10.1306/819A424C-16C5-11D7-8645000102C1865D

Hayes, G.P., Moore, G.L., Portner, D.E., Hearne, M., Flamme, H., Furtney, M., & Smoczyk, G.M. (2018). Slab2, a comprehensive subduction zone geometry model. Science 362, 58–61. https://doi.org/10.1126/science.aat4723

Kavyani-Sadr, K., Rahimi, B., Khatib, M.M., & Kim, Y.-S. (2022). Assessment of open spaces related to Riedel-shears dip effect in brittle shear zones. Journal of Structural Geology 154, 104486. https://doi.org/10.1016/j.jsg.2021.104486

Kusumawati, D., Sahara, D. P., Puspito, N. T., Daryono, M. R., Nugraha, A. D., Sadly, M., Prayitno, B. S., Daryono, D., Heryandoko, N., & Rohadi, S. (2025). Stress orientation at the Palu-koro fault, Indonesia, based on regional focal mechanism data. *Advances in Science, Technology & Innovation*, *Springer*.

Laske, G., Masters, G., Ma, Z., & Pasyanos, M. (2013). Update on CRUST1.0 - A 1-degree Global Model of Earth's Crust EGU2013-2658.

Natawidjaja, D.H., Daryono, M.R., Prasetya, G., Udrekh, Liu, P.L.-F., Hananto, N.D., Kongko, W., Triyoso, W., Puji, A.R., Meilano, I., Gunawan, E., Supendi, P., Pamumpuni, A., Irsyam, M., Faizal, L., Hidayati, S., Sapiie, B., Kusuma, M.A., & Tawil, S. (2021). The 2018 Mw7.5 Palu 'supershear' earthquake ruptures geological fault's multisegment separated by large bends: results from integrating field measurements, LiDAR, swath bathymetry and seismic-reflection data. Geophysical Journal International 224, 985–1002. https://doi.org/10.1093/gji/ggaa498

Octhav, A., Sahara, D.P., & Kusumawati, D. (2025). The principal stress analysis of Matano Fault segment from focal mechanism inversion. IOP Conf. Ser.: Earth and Environmental Science 1472, 012013. https://doi.org/10.1088/1755-1315/1472/1/012013

Oppenheimer, D.H., Reasenberg, P.A., & Simpson, R.W. (1988). Fault plane solutions for the 1984 Morgan Hill, California, Earthquake Sequence: Evidence for the state of stress on the Calaveras Fault. Journal of Geophysical Research: Solid Earth 93, 9007–9026. https://doi.org/10.1029/JB093iB08p09007

Patria, A., Natawidjaja, D.H., Daryono, M.R., Hanif, M., Puji, A.R., & Tsutsumi, H. (2023). Tectonic landform and paleoseismic events of the easternmost Matano fault in Sulawesi, Indonesia. Tectonophysics 852, 229762. https://doi.org/10.1016/j.tecto.2023.229762

PUSGEN (National Center for Earthquake Studies of Indonesia) (2017). Indonesia's Earthquake Source and Hazard Map (In Bahasa Indonesia). Indonesia: Research and Development Agency of Ministry of Public Work and Housing

Ragan, D.M. (1973). Structural Geology: An Introduction to Geometrical Techniques. Wiley.

Riedel, W. (1929). Zur Mechanik geologischer Brucherscheinungen. Zur Mechanik Geologischer Brucherscheinungen 354–368.

Roy, A., Roy, N., Saha, P., & Mandal, N. (2021). Factors Determining Shear-Parallel Versus Low-Angle Shear Band Localization in Shear Deformations: Laboratory Experiments and Numerical Simulations. Journal of Geophysical Research: Solid Earth 126, e2021JB022578. https://doi.org/10.1029/2021JB022578

Sibson, R. (1974). Frictional constraints on thrust, wrench and normal faults. Nature 249, 542–544. https://doi.org/10.1038/249542a0

Silver, E.A., McCaffrey, R., & Smith, R.B. (1983). Collision, rotation, and the initiation of subduction in the evolution of Sulawesi, Indonesia. Journal of Geophysical Research: Solid Earth 88, 9407–9418. https://doi.org/10.1029/JB088iB11p09407

Socquet, A., Simons, W., Vigny, C., McCaffrey, R., Subarya, C., Sarsito, D., Ambrosius, B., & Spakman, W. (2006). Microblock rotations and fault coupling in SE Asia triple junction (Sulawesi, Indonesia) from GPS and earthquake slip vector data. Journal of Geophysical Research: Solid Earth 111. https://doi.org/10.1029/2005JB003963

Uieda, L., & Wessel, P. (2017). A modern Python interface for the Generic Mapping Tools. Presented at the 2017 AGU Fall Meeting, AGU.

Wang, H., Liu, M., Ye, J., Cao, J., & Jing, Y. (2017). Strain partitioning and stress perturbation around stepovers and bends of strike-slip faults: Numerical results. Tectonophysics 721, 211–226. https://doi.org/10.1016/j.tecto.2017.10.001

Yu, H., Kao, H., Wang, B., & Visser, R. (2022). Long-Term Fluid Injection Can Expedite Fault Reactivation and Development: Riedel Shear Structures Illuminated by Induced Earthquakes in Alberta, Canada. Journal of Geophysical Research: Solid Earth 127, e2022JB025126. https://doi.org/10.1029/2022JB025126

Zelst, I., Crameri, F., Pusok, A., Glerum, A., Dannberg, J., & Thieulot, C. (2021). 101 Geodynamic modelling: How to design, carry out, and interpret numerical studies. https://doi.org/10.5194/se-2021-14

Zheng, T., Qiu, Q., Lin, J., & Yang, X. (2023). Raised potential earthquake and tsunami hazards at the North Sulawesi subduction zone after a flurry of major seismicity. Marine and Petroleum Geology 148, 106024. https://doi.org/10.1016/j.marpetgeo.2022.106024

SAŽETAK

Modeliranje utjecaja lateralnog opterećenja na povijesne "strike-slip" sustave rasjeda: primjer iz Palu-koro Matano rasjeda, Indonezija

Rasjedi Palu–koro i Matano tvore glavni povijeni "strike-slip" sustav rasjeda u središnjem dijelu Sulawesi, Indonezija, te prihvaćaju značajne deformacije kore povezane s regionalnim pokretima tektonskih ploča. U ovoj studiji istražen je mehanički odgovor ovog rasjednog sustava koristeći trodimenzionalno numeričko modeliranje kako bi se procijenili utjecaji različitih lateralnih opterećenja na pomak rasjeda i raspodjelu naprezanja. Dirichletovi (brzina pomaka) granični uvjeti, izvedeni iz regionalnih brzina kretanja tektonskih ploča, primijenjenu su na model na x-lice, y-lice, te u kombiniranim konfiguracijama x- i y-lica. Modeli s čistim opterećenjima na x-licu ili y-licu stvaraju lateralne obrasce klizanja koji su mehanički kompatibilni s idealiziranom kinematikom Riedelovih smičnih zona; međutim, smjer klizanja razlikuje se od današnjeg tektonskog kretanja Palu–koro i Matano rasjeda. Suprotno tome, modeli w kombiniranim graničnim uvjetima reproduciraju karakteristike prvog reda promatranog ponašanja rasjeda. Konkretno, slučajevi s dominantno lateralnim opterećenjem na x-licu (npr. 70% x-lice i 30% y-lice) proizvode pretežito lijeve pomake duž oba rasjeda i više koncentracije klizanja duž Palu–koro rasjeda, što je u skladu s tektonskim i geodetskim opažanjima. Kombinirani model opterećenja također pokazuje suptilnu rotaciju orijentacije maksimalnog glavnog naprezanja od ZNZ-IJI duž Palu–koro rasjeda do SI-JZ duž Matano rasjeda, što kvalitativno odgovara orijentacijama naprezanja izvedenim iz fokalnih mehanizama inverzije. Općenito, rezultati ukazuju da kombinirano regionalno lateralno opterećenje, s dominantnim sjever-jug lateralnim pomakom, pruža prihvatljiv mehanički okvir za razumijevanje lokaliziranih deformacija i rotacije osi naprezanja unutar Palu–koro–Matano rasjednog sustava.

Ključne riječi:
povijeni "strike-slip", rasjedno lateralno klizanje, rastezno lateralno klizanje, Matano rasjed, numeričko modeliranje, Palu-koro rasjed, Riedelovo smicanje

Author's contribution

Dian Kusumawati (Dr., expertise in seismology and numerical modelling): performed and conceived the study, conceptualization, wrote the original draft. **David P. Sahara** (Dr. rer. nat., expertise in seismology and geomechanics): performed supervision and formal analysis, review and editing the draft, project administration. **Nanang T. Puspito** (Dr., seismology Professor): performed supervision, formal analysis, funding acquisition, and reviewed the draft. **Mudrik R. Daryono** (Dr., expertise in geology): performed supervision, formal analysis, and reviewed the draft. **Andri D. Nugraha** (Dr., seismology Professor): data curation. **Andrean V. H. Simanjuntak** (Dr., expertise in seismology): perfomed visualization and reviewed the draft. **Maulidia Ain Bening** (Meng., expertise in numerical modelling): performed software methodology. **Faiz Muttaqy** (Dr., expertise in seismology and tomography): performed supervision and reviewed the draft.
All authors have read and agreed to the published version of the manuscript.